SKB

TECHNICAL REPORT 91-11

Impact from the disturbed zone on nuclide migration – a radioactive waste repository study

Akke Bengtsson[1], Bertil Grundfelt[1], Anders Markström[1], Anders Rasmuson[2]

[1] KEMAKTA Konsult AB
[2] Chalmers Institute of Technology

January 1991

SVENSK KÄRNBRÄNSLEHANTERING AB
SWEDISH NUCLEAR FUEL AND WASTE MANAGEMENT CO

BOX 5864 S-102 48 STOCKHOLM

TEL 08-665 28 00 TELEX 13108 SKB S
TELEFAX 08-661 57 19

IMPACT FROM THE DISTURBED ZONE ON NUCLIDE MIGRATION - A RADIOACTIVE WASTE REPOSITORY STUDY

Akke Bengtsson[1], Bertil Grundfelt[1], Anders Markström[1], Anders Rasmuson[2]

1 KEMAKTA Konsult AB
2 Chalmers Institute of Technology

January 1991

Impact from the disturbed zone on nuclide migration - a radioactive waste repository study

by:
Akke Bengtsson [1]
Bertil Grundfelt [1]
Anders Markström [1]
Anders Rasmuson [2]

[1] KEMAKTA Konsult AB
[2] Chalmers Institute of Technology

January 1991

TABLE OF CONTENTS

SUMMARY

During excavation of tunnels in crystalline rock a permeable zone is developed around the tunnel wall periphery - a disturbed zone. In the present report both numerical and analytical calculations have been performed to evaluate the importance of the disturbed zone for radionuclide migration from a final storage of radioactive waste.

The magnitude of the groundwater flow rate within the disturbed zone depends on the orientation of the repository tunnels relative the regional flow direction. The largest flow rate increase is obtained when the regional flow direction is parallel to the tunnel principal axis. In this case the magnitude of the flow rate increase is approximately proportional to the permeability contrast between the disturbed zone and the undisturbed rock. For flow transverse the tunnel axis the flow rate increase is limited to maximum twice the flow in the undisturbed rock.

In the numerical groundwater flow calculations, particles have been released from the positions of the canisters below the tunnel floor. The results show that at least some of the pathways from the canisters reach to the disturbed zone when the tunnel axis is oriented parallel to the regional flow.

The radionuclide migration calculations show that the nuclide transport velocity within the disturbed zone might be faster than the transport velocity in the undisturbed rock.

Finally, it is concluded that there is a need for a more accurate study of the modelling strategy for the near-field in order to account for the release of radionuclides to the disturbed zone.

1 BACKGROUND

According to (Pusch 1990), the part of the rock that is adjacent to the excavated tunnels - in this context called the disturbed zone, has an increased permeability relative to the surrounding rock. This permeable zone is developed during excavation of tunnels partly through the mechanical work but also because of rock stress redistribution.

I this report examples are given of the effect of the disturbed zone on:

- Groundwater flow within the repository area
- Transportation of nuclides from a canister to an adjacent fracture zone

2 GROUNDWATER FLOW WITHIN THE REPOSITORY AREA

2.1 Considerations from potential-flow theory

A local increase of the hydraulic conductivity in a water-bearing rock exaggerates the groundwater flow rate in the domain. The water that normally passes by the area, will now flow through the domain. The flow-rate increase within the area depends on the increase of hydraulic conductivity, the angle between the flow direction within and outside the high-permeability area, and the geometry of the conductive area. Larger extension of the conductive area in the flow direction implies higher flow increase within the permeable area compared to the undisturbed flow.

In Figure 2.1 and Figure 2.2 it is illustrated how the groundwater pressure distribution is changed in an area comprising a prolate spheroid with a higher hydraulic conductivity compared to surrounding media for flow along and perpendicular to the principal axis of the ellipsoid. At large distance from the prolate spheroid the potential is proportional to the y-coordinate, i.e. the potential profiles are parallel in an undisturbed media (Carslaw & Jaeger,1959).

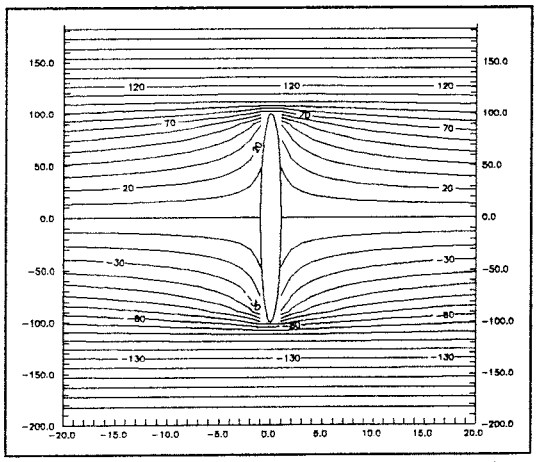

Figure 2.1 Isopotentials around a prolate spheroid with an increased permeability of a factor 10^4 relative to surrounding medium. Potential gradient parallel to spheroid principal axis.

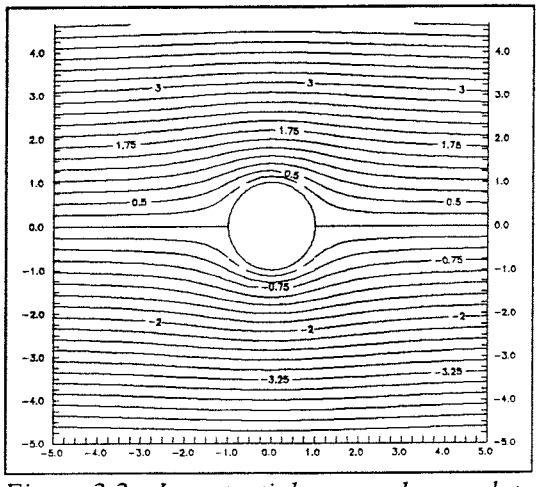

Figure 2.2 Isopotentials around a prolate spheroid with an increased permeability of a factor 10^4 relative to surrounding medium. Gradient perpendicular to spheroid principal axis.

For a flow in a medium with the conductivity K directed perpendicular to an infinitely long cylinder with the conductivity K' a flow rate is obtained (m^3/m^2,s) per meter cylinder Q'. This flow can be compared with the flow through the same area under undisturbed conditions Q:

$$\frac{Q'}{Q}=\frac{2K'}{K'+K}$$

The theoretical maximum for the flow rate increase is a factor 2, in the case of an infinitely permeable tunnel. Some combinations of Q'/Q and K'/K are shown in Table 2.1.

Table 2.1 Flow rate increase for flow perpendicular to a cylinder

K'/K	Q'/Q
∞	2.0
1.0	1.0
0.0	0.0

The flow conditions in a cylinder for flow parallel to the cylinder axis are more difficult to calculate. The above mentioned approach using a prolate spheroid, however, is a reasonable approximation of the conditions. In the same way we denote a flow Q' (m^3/m^2,s) in the a prolate spheroid with the conductivity K' and a corresponding flow rate Q in the undisturbed rock with the conductivity K. Then the following equation is given:

$$\frac{Q'}{Q}=\frac{\frac{K'}{K}}{1+A_0(\frac{K'}{K}-1)}$$

Where:

$$e=\sqrt{1-\frac{b^2}{a^2}}$$

$$A_0=\frac{1-e^2}{e^3}\left[\frac{1}{2}\ln\left(\frac{1+e}{1-e}\right)-e\right]$$

For small b/a, A_0 rapidly approaches:

$$A_0=\frac{b^2}{a^2}\left[\ln\left(\frac{2a}{b}\right)-1\right]$$

Some combinations of Q'/Q and K'/K are presented in Table 2.2. A few combinations regarding length, width and permeability contrast are shown in table 2.3. By studying the numbers in Table 2.3 it can be concluded that the flow rate in this case can increase some orders of magnitude.

Table 2.2 Flow rate increase through a prolate spheroid, parallel to the hydraulic gradient

K'/K	Q'/Q
∞	$1/A_0$
1.0	1.0
0.0	0.0

Table 2.3 Flow increase through a prolate spheroid, approximately size of a single KBS-3 repository tunnel. Hydraulic gradient parallel to the spheroid principal axis.

	Q'/Q	
K'/K	b/a=0.01 $A_0=4.3\cdot10^{-4}$	b/a=0.02 $A_0=1.44\cdot10^{-3}$
10.0	9.96	9.87
100.0	95.9	87.5
1000.0	699.0	410.0
∞	$2.33\cdot10^{3}$	694.0

In Figure 2.3 and Figure 2.4 it is illustrated how magnitude and direction of the flow inside a spheroid varies as a function of the angle between the prolate spheroid principal axis and the undisturbed flow in the undisturbed surrounding media. The calculations have been performed for a prolate spheroid 500 m long with a maximum diameter at the spheroid centre of 10 m, which approximately corresponds to a single KBS-3 repository tunnel including a disturbed zone (equivalent length and volume).

As can be seen from Figure 2.3, the magnitude of the flow rate inside the ellipsoid is relatively insensitive to variations of the angle between the ellipsoid principal axis and the direction of the undisturbed flow outside the tunnel when the permeability is slightly decreased. However, at an angle almost perpendicular to the length axis the flow is considerably decreased compared to the maximum value for flow directions parallel to the length axis.

An effective conductivity can be calculated in the case where the conductivity differs in different parts of a cross-section. When the flow is parallel through different materials with the conductivities K' and K'' and the cross-sectional areas A' and A'' respectively, the effective conductivity is given by:

$$K_{eff}=\frac{K'\cdot A'+K''\cdot A''}{A'+A''}$$

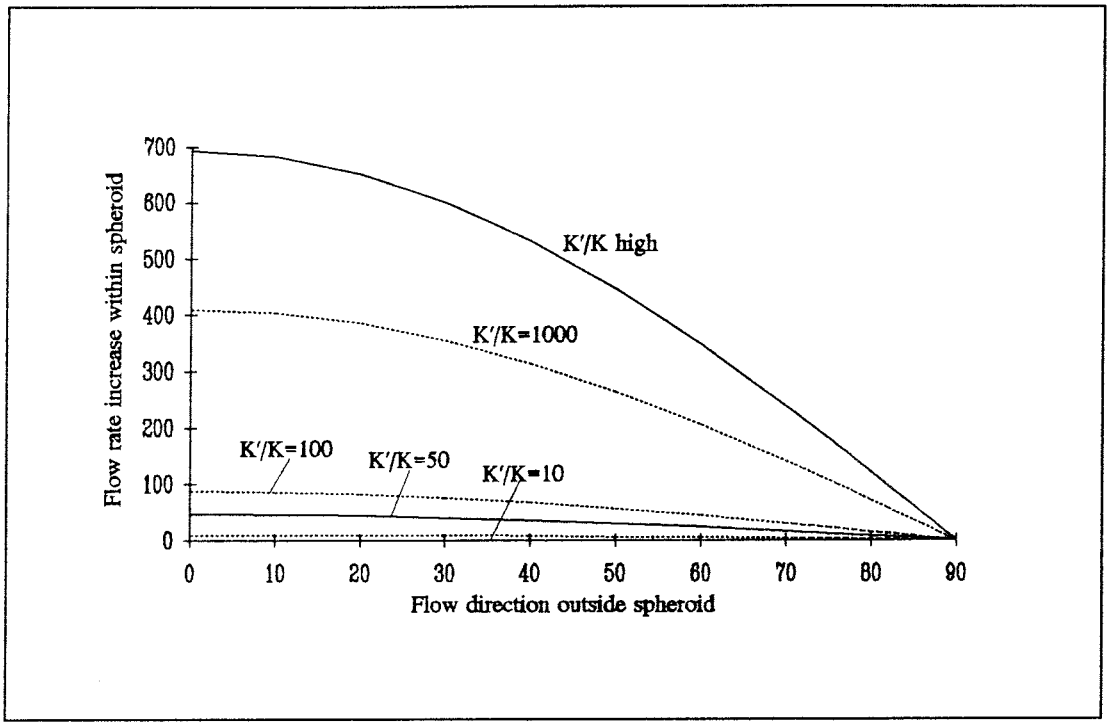

Figure 2.3 Flow rate increase within a prolate spheroid (b/a=0.02) as a function of the hydraulic gradient direction.

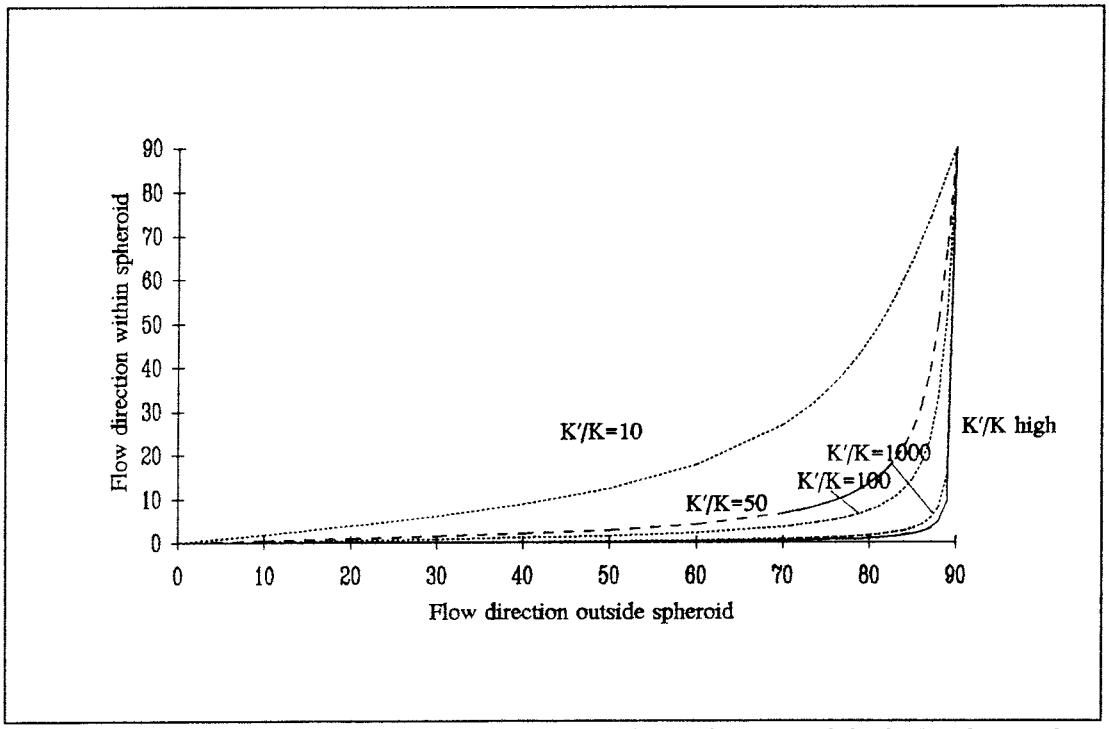

Figure 2.4 Flow direction within a prolate spheroid as a function of the hydraulic gradient direction.

This expression could be applicable to a tunnel with a permeable disturbed zone surrounding a relatively impermeable clay backfill. On the other hand, if an impervious zone surrounds a permeable tunnel backfill, the flow rate in the tunnel would be limited by the flow rate through the impervious zone and the expression above would lose its validity.

In the case defined in Chapter 3 for the transport calculations, the effective conductivity of the tunnel including the disturbed zone is a factor between 30 and 50 times higher than the conductivity of the surrounding rock. The higher value, which is valid for flow along the tunnel, has been included in Figures 2.3 and 2.4.

The flow rate in the rock mass, in the vicinity of the disturbed zone, i.e. at the canister positions, is not dramatically affected. For b/a=0.02 (equivalent with the case in the right column of Table 2.3) and K'/K=50, a flow increase of less then 50 % compared with the undisturbed flow is obtained close to the tunnel ends. About 90% of the undisturbed flow is obtained at the mid section of the tunnel (see Figure 2.5).

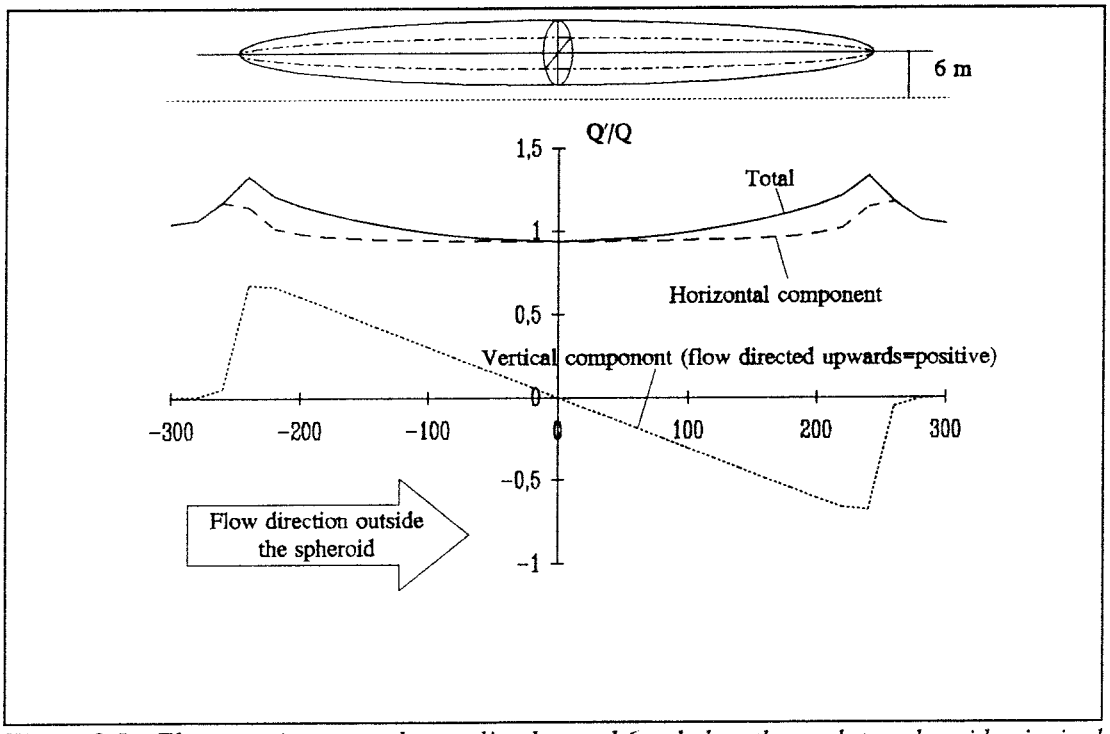

Figure 2.5 Flow rate increase along a line located 6 m below the prolate spheroid principal axis where a=250m, b=5m and K'/K=50. The hydraulic gradient is parallel to the spheroid.

The KBS-3 repository concept consists of tunnels positioned parallel to each other at an internal distance of 25 m (KBS-3, 1983). The effect of multiple tunnels has not been studied, but the following quantitative conclusions can be drawn:

When the flow is perpendicular to the tunnel the interference between the tunnels is limited. For flow parallel to the tunnel axis the water collection area is much larger and the flow rate in the tunnel is hence limited by geometrical constraints.

2.2 Numerical modelling

2.2.1 General

The main purpose of the modelling is to illustrate the effect of a disturbed zone located around the tunnel periphery on the hydrology at a potential repository. Calculations are performed for a 3-dimensional, substantially simplified representation of a single repository tunnel located 500 m below the ground surface in a bedrock, which with the exception of some significant fracture zones with a different permeability, is assumed to be homogenous. A simple scenario has been set up to give a rough qualitative picture of the effect from the different phenomena involved.

The generic 3-dimensional model comprises a repository tunnel (500 m) surrounded by a 1 m wide high-permeable disturbed zone adjacent to the tunnel periphery, Figure 2.10. Flowpaths have been recorded from a number of release points located 2 m below the tunnel floor. The general flow field direction and the hydraulic conductivity of the disturbed zone have been varied.

The modelling is made at two scales, a regional and a local scale. The main purpose of the regional modelling is to deliver boundary conditions to the local model. The tunnel and the disturbed zone are not included in the regional model.

The calculations have been performed assuming steady-state conditions, and using the finite-element method.

2.2.2 Regional model

Description of the geometry and modelling assumptions

The horizontal extent of the model is 500x2000m. The outer vertical boundaries have been assigned no-flow conditions. The bottom surface boundary located at z=-2000m has also been assigned no-flow boundary conditions.

The driving force in the model is a monotonously slanting groundwater surface. The gradient is set to 1%. The topmost elevation of the groundwater table is z=20m, and the lowest level is z=0m. The top surface of the model has been assigned atmospheric pressure.

The element mesh comprises totally 23712 elements and 26622 nodal points, see Figure 2.6.

Three cases have been calculated utilizing the regional model. The undisturbed flow is calculated in all three cases, i.e. neither the repository tunnel nor the disturbed zone is modelled in the regional model.

In Case R1 a completely homogenous bedrock is assumed. In Case R2 the effect of having two vertical zones located upstream and downstream of the potential repository is illustrated. The distance between the two zones is 300m. Case R3 elucidates the effect of a horizontal zone located at the level of z=300m. Parameter values used (hydraulic conductivity) are shown in Table 2.4.

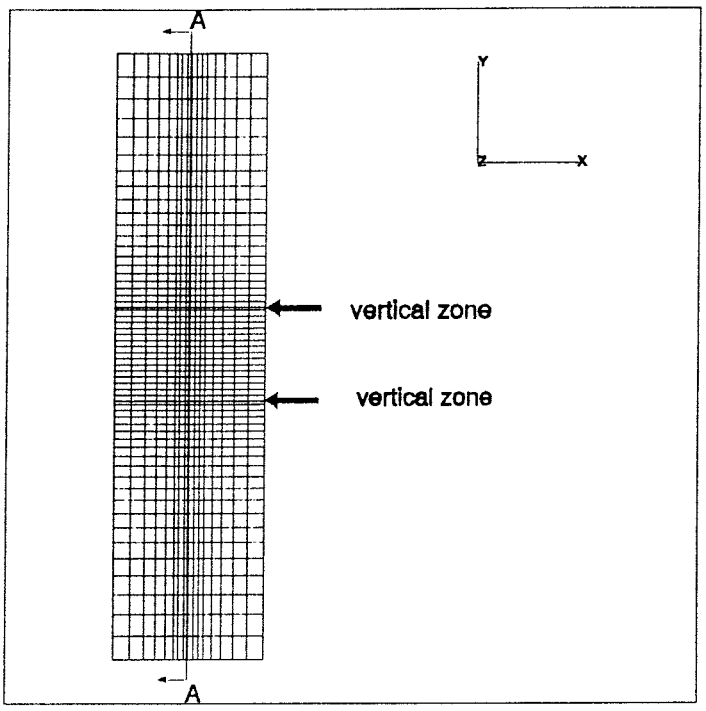

Figure 2.6 Horizontal view of the finite element mesh of the regional model.

Table 2.4 Material properties (hydraulic conductivity) for Case 1-3 in the regional model

	Case 1 [m/s]	Case 2 [m/s]	Case 3 [m/s]
$K_{rock\ mass}$	10^{-10}	10^{-10}	10^{-10}
$K_{vertical\ zone}$	-	10^{-7} (10m)	10^{-7} (10m)
$K_{horizontal\ zone}$	-	-	10^{-5} (100m)

Results

The groundwater flow potential distribution for Cases R1-R3 is plotted on a vertical cross-section in Figures 2.7-2.9. The vertical cross-section is located at the centre of the potential repository parallel to the direction of the main flow gradient, see cut A-A in Figure 2.6. The position of the local model is indicated in the figures, although it is not explicitly included in the regional model.

In Figure 2.7 the potential distribution is shown for Case R1 under conditions of homogenous rock mass. The flow, which is perpendicular to the isopotential lines, in the repository area has a predominant horizontal component. Nevertheless a flow component directed upwards is detectable at the upstream section of the repository area and a downward directed component at the downstream section of the repository.

In Case R2, Figure 2.8, the two vertical zones are included increasing the potential drop between the vertical zones while the potential drop outside the zones is decreased. The reason for this is that the relatively high conductivity in the vertical zones leads to a lower vertical flow resistance, thus

the potentials at the ground surface is transferred far down in the domain without being considerably reduced.

Case R3, Figure 2.9, shows that the comparably high permeability contrast between the rock mass and the horizontal zone, a factor 10^5, in combination with zone continuity over the whole modelled domain has yielded an extremely low hydraulic gradient at the level of the repository.

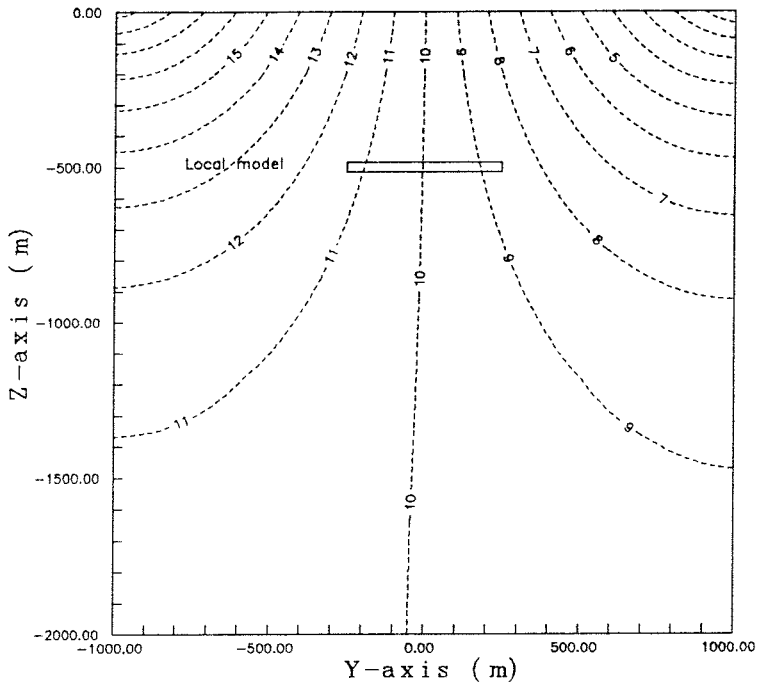

Figure 2.7 Isopotentials (m) in a vertical cross-section through the repository area, Case R1 regional model. The position of the local model is indicated in the figure.

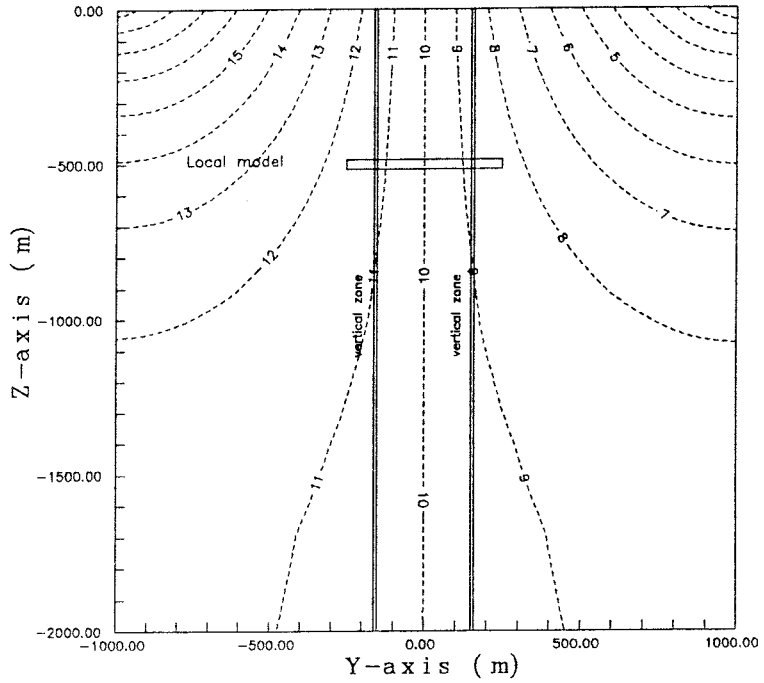

Figure 2.8 Isopotentials(m) in a vertical cross-section through the repository area, Case R2 regional model.

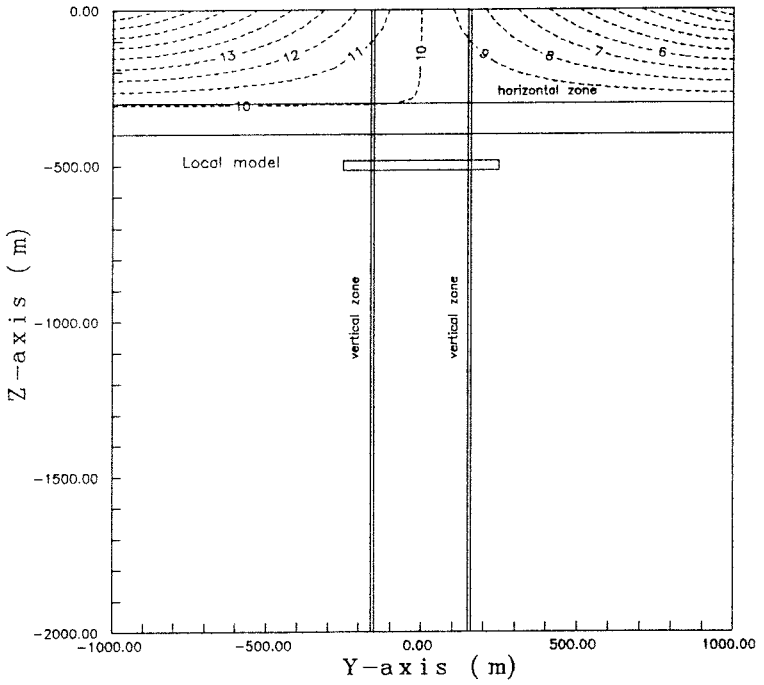

Figure 2.9 Isopotentials(m) in a vertical cross-section through the repository area, Case R3 regional model. The position of the local model is indicated in the figure.

2.2.3 Local model

Description of geometry and modelling assumptions

The model describes a 500 m long repository tunnel with a cross-sectional area of 3.3x4.5m. The geometry of the tunnel is in the model simplified to the shape of a rectilinear block, see Figure 2.10. The disturbed zone is modelled as a 1 m thick shell around the tunnel. The distance between the centre of the tunnel and the model boundary is 15 m, which is judged to be sufficient to be outside of the influence radius of the disturbed zone. The extent of the model is 30x500x30m. The tunnel backfill(sand/bentonite) has been assigned the same permeability as the surrounding rock mass.

The boundary conditions in the local model is derived from the calculation results of the regional model, see table 2.5.

The element mesh consists of 18150 elements and 21744 nodal points, see Figure 2.11.

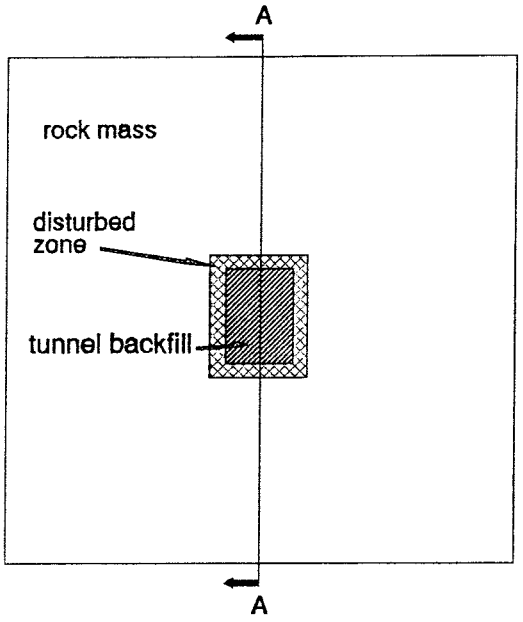

Figure 2.10 *Vertical cross-section through the local model(30x30m). The position of the local model is indicated in the figure.*

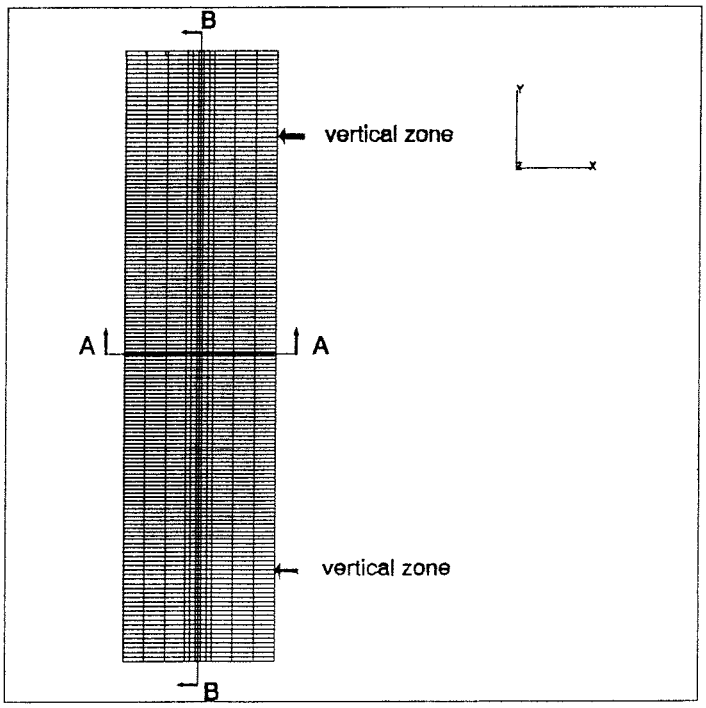

Figure 2.11 Horizontal view of the finite element mesh in the local model. For reasons of clarity the x-axis scale has been enlarged a factor 4. Cut A-A is shown in Figure 2.10.

The following cases have been studied;

Case L1 describes the flow in the repository area under undisturbed conditions, i.e. the disturbed zone is assigned the same permeability as the rock mass.

In Case L2 the influence of the disturbed zone on the flow field at the repository area is studied assuming homogenous rock mass.

Case L3 describes the flow under undisturbed conditions with two vertical zones intersecting in the repository area. The vertical zones has been assigned a hydraulic conductivity of $K=10^{-7}$m/s.

Case L4 elucidates the effect of shortcircuiting the groundwater flow through the two vertical zones and the disturbed zone. The permeability contrast between the rock mass and the disturbed zone is a factor 10^4.

In Case L5 the effect of a lower permeability contrast(10^2) between rock mass/disturbed zone is studied, compare with Case L4.

Case L6 describes the effect of the main flow directed perpendicular to the tunnel centre axis. This is achieved by turning the local model 90° inside the regional model when setting the boundary conditions. Remaining assumptions are equal to Case L4.

Case L7 throws light upon the effect of introducing a highly permeable horizontal zone located above the repository area.

The different calculation cases are summarized in table 2.5 below.

Table 2.5 Material properties(hydraulic conductivity) and boundary conditions for Case 1-7 in the local model.

	L 1 [m/s]	L 2 [m/s]	L 3 [m/s]	L 4 [m/s]	L 5 [m/s]	L 6 [m/s]	L 7 [m/s]
$K_{rock\ mass}$ [1)]	10^{-10}	10^{-10}	10^{-10}	10^{-10}	10^{-10}	10^{-10}	10^{-10}
$K_{disturbed\ zone}$	-	10^{-6}	-	10^{-6}	10^{-8}	10^{-6}	10^{-6}
$K_{vertical\ zone}$	-	-	10^{-7}	10^{-7}	10^{-7}	10^{-7}	10^{-7}
$K_{horiz.\ zone}$	-	-	-	-	-	-	10^{-5}
t-axis[2)]	p	p	p	p	p	pe	p
boundary cond.[3)]	R 1	R 1	R 2	R 2	R 2	R 2	R 3

1) The same hydraulic conductivity is used for the tunnel backfill

2) Direction of tunnel principal axis relative to the direction of the main hydraulic gradient; p=parallel, pe=perpendicular

3) Boundary conditions have been transferred as groundwater pressures from the regional model Case R1-R3

Results

Figure 2.12-2.17 show the groundwater potential distribution for calculation case 1-6. The calculated isopotentials for Case 7 is not presented as the hydraulic gradients in the repository area are very low, i.e. in the same order of magnitude as the numerical precision of the finite element model.

The figures show the groundwater potential distribution (metres of water head) on a vertical cross-section positioned at the centre of the tunnel and parallel to the regional hydraulic gradient, cut A-A in Figure 2.10 and cut B-B i Figure 2.11. For reasons of clarity the scale on the vertical axis has been expanded a factor 4 relative to the scale of the horizontal axis.

Case L1, Figure 2.12, illustrates the calculated groundwater potential distribution within the repository area under undisturbed conditions and homogenous rock mass.

In Case L2, Figure 2.13, the impact from the disturbed zone comprising a permeability contrast of 10^4 between rock mass and the disturbed zone is illuminated. It can be concluded that the most obvious disturbance on the general flow field pattern, is seen in the upper part of the disturbed zone.

Case L3, Figure 2.14, illustrates the increase in potential difference and potential drop in the repository area when including the two vertical zones in the model, compare with Case L1, Figure 2.12. The groundwater potentials at the ground surface are transported via the relatively highly permeable zones far down into the domain without being significantly reduced.

Case L4, Figure 2.15, describes the impact from the disturbed zone having a relatively high permeability contrast (10^4) between the disturbed zone and the rock mass. In the critical area beneath the lower part of the disturbed zone a local hydraulic gradient directed upwards is formed in the upstream portion of the repository and a downward directed gradient is formed at the downstream section of the tunnel.

The results in Case L5, Figure 2.16, is similar to the results obtained in Case L1, i.e. the regional flow pattern is predominant. The lower contrast between rock mass and disturbed zone (10^2) implies less influence from the disturbed zone compared to Case L4.

In Figure 2.17, Case L6, the potential distribution for a repository tunnel located perpendicular to the regional flow is presented. The interference from the disturbed zone on the regional flow is in this case very limited. It should be pointed out that the vertical zones have been indicated in the figure although they in Case L6 have not been included in the local model.

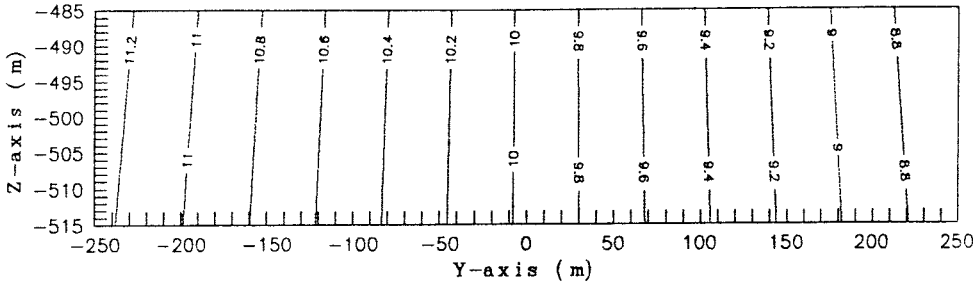

Figure 2.12 Isopotentials (m) on a vertical cross-section along the centre of the repository tunnel, Case L1 local model.

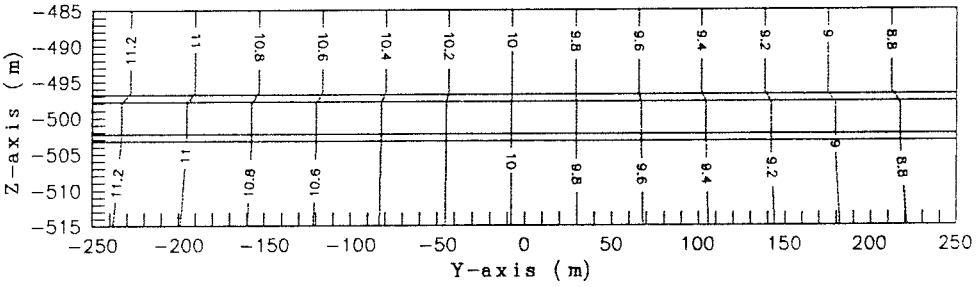

Figure 2.13 Isopotentials (m) on a vertical cross-section along the centre of the repository tunnel, Case L2 local model.

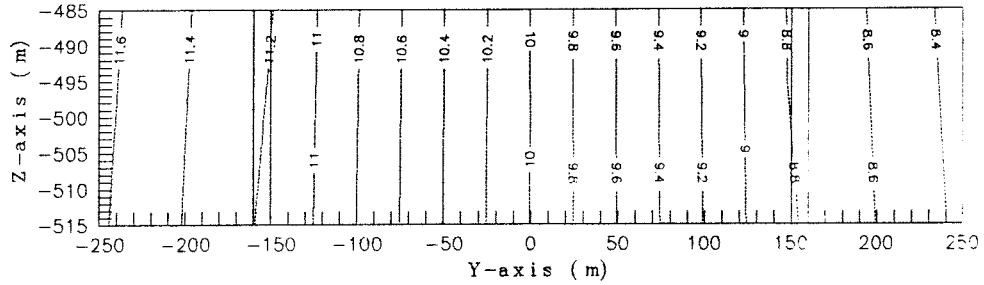

Figure 2.14 Isopotentials (m) on a vertical cross-section along the repository tunnel, Case L3 local model.

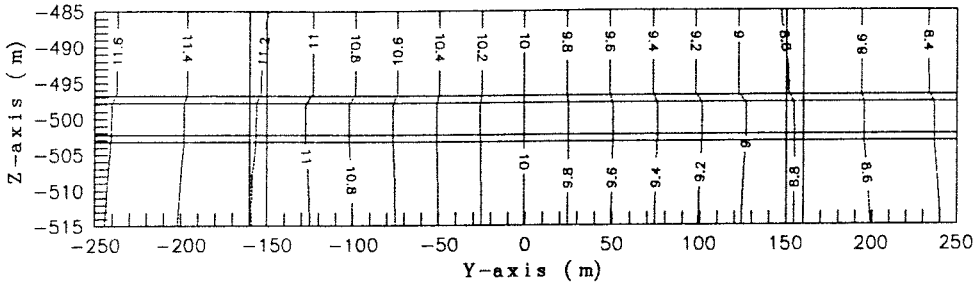

Figure 2.15 Isopotentials (m) on a vertical cross-section along the centre of the repository tunnel, Case L4 local model.

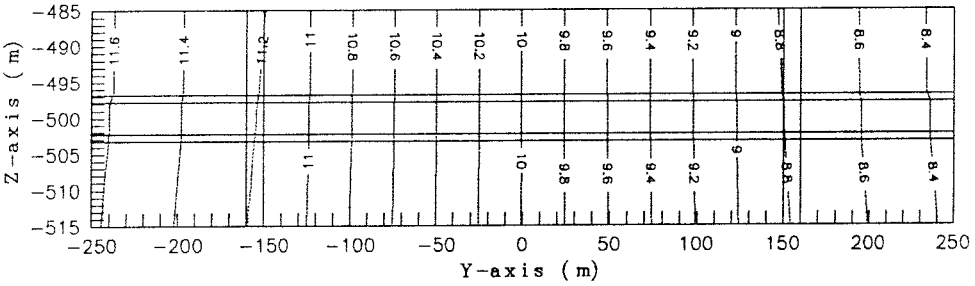

Figure 2.16 Isopotentials (m) on a vertical cross-section along the centre of the repository tunnel, Case L5 local model.

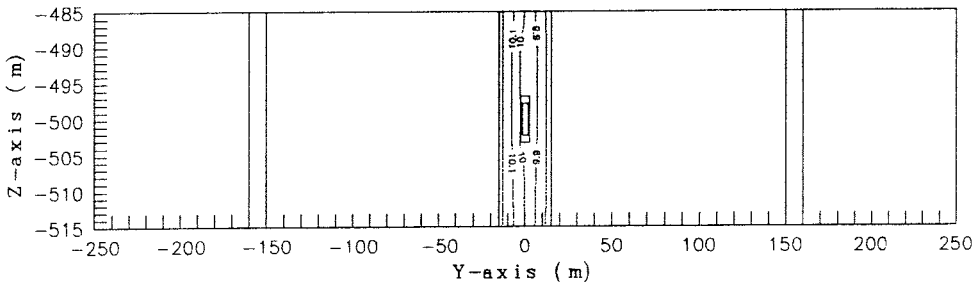

Figure 2.17 Isopotentials (m) on a vertical cross-section perpendicular to repository tunnel principle axis, Case L6 local model.

Five particles have been released in each calculation case to illustrate how the resulting pathways from the waste canisters vary in the different calculation cases, Figures 2.18-2.23. The particle release points are located beneath the tunnel centre line at a level of 1 m below the disturbed zone, i.e. 2 m below the tunnel floor. The elevation of the release points corresponds approximately to the level of the top of the canisters. For reasons of clarity the scale on the vertical axis (z-axis) has been exaggerated by a factor 4 relative to the horizontal axis scale. The particles have been followed to the point where they enter the downstream vertical fracture zone.

Case L1, Figure 2.18, illustrates the pathlines following the regional flow pattern for undisturbed conditions.

In Case L2, Figure 2.19, the particles follow the regional flow field until the disturbed zone is reached. From here the particles are diverted via the disturbed zone out to the downstream vertical boundary of the model. The vertical flow component is greater than in Case L1 because the disturbed zone acts as a water collector creating more horizontal pathways compared with Case L1.

Case L3, Figure 2.20, illustrates the effect of introducing vertical zones in the model where the disturbed zone is omitted, i.e. undisturbed conditions. All pathlines are released to the downstream located vertical zone, and further upwards to the upper boundary of the model.

In Case L4, Figure 2.21, the permeability contrast between rock mass and the disturbed zone leads to an inflow at the upstream section of the repository and an outflow at the downstream section of the repository. This causes particles released in the upstream part of the repository area to go up into the disturbed zone. The relatively high permeability contrast between rock mass and the disturbed zone leads to an effective shortcircuiting of the flow between the vertical zones. Due to the stagnation point at the downstream end of the tunnel, an overpressure is formed which pushes the particles slightly downwards in the downstream fracture zone. Because of the exaggerated vertical scale, the effect looks more significant in Figure 2.22 than it is. Also, particles started in positions located downstream the repository centre are pressed downwards in the direction towards to bottom surface boundary where they exit the model.

Case L5, Figure 2.21, is a compromise between Case L3 and Case L4 where the contrast between rock mass and the disturbed zone is a factor 100 times less than the contrast in Case L4. The results show that all pathlines at the beginning follow the regional flow pattern, compare with Case L3. At the intersection between the downstream located vertical zone and the disturbed zone the particles are led vertically upwards to an elevation approximately 1 m above the tunnel roof. At this point the regional flow field becomes predominant again. All particles are led out into the rock mass and towards the vertical boundary of the model.

In Case L6, Figure 2.23, where the repository is positioned perpendicular to the regional hydraulic gradient, just a minor disturbance on the regional flow field and on the trajectory is obtained. Directly after the release the particle is pressed downwards. Afterwards the pathline follows the regional flow field towards the vertical boundary. It should be pointed out that the vertical zones for reasons of clarity have been indicated in the figure despite that they are not included in the model for Case L6.

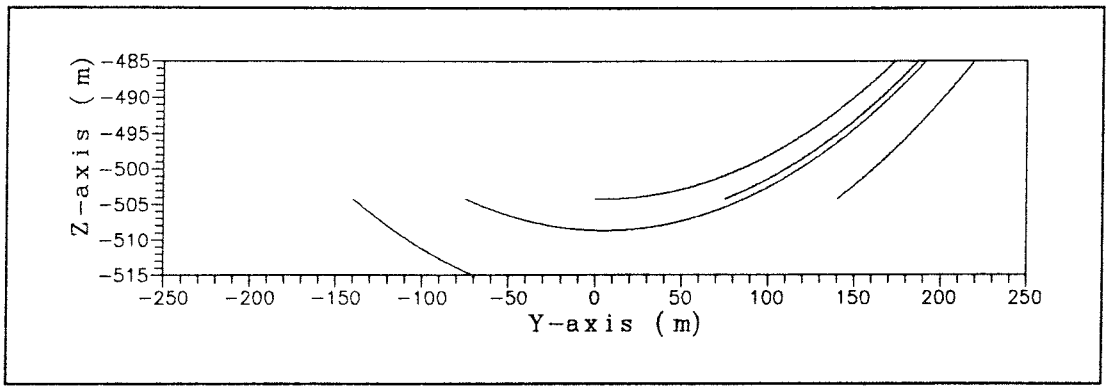

Figure 2.18 Pathlines released at the elevation of the canisters, Case L1 local model.

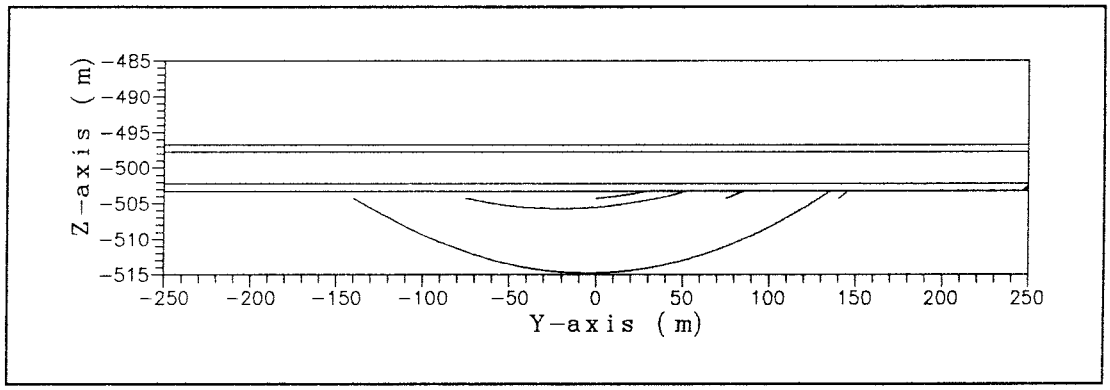

Figure 2.19 Pathlines released at the elevation of the canisters, Case L2 local model.

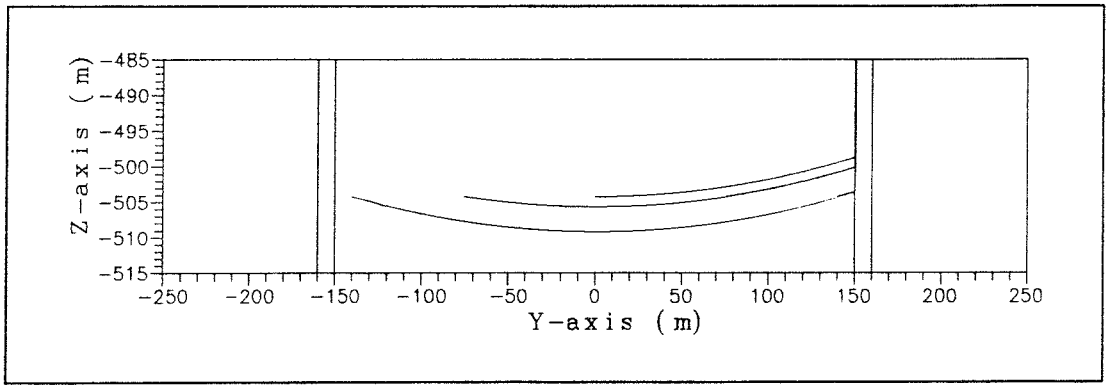

Figure 2.20 Pathlines released at the elevation of the canisters, Case L3 local model.

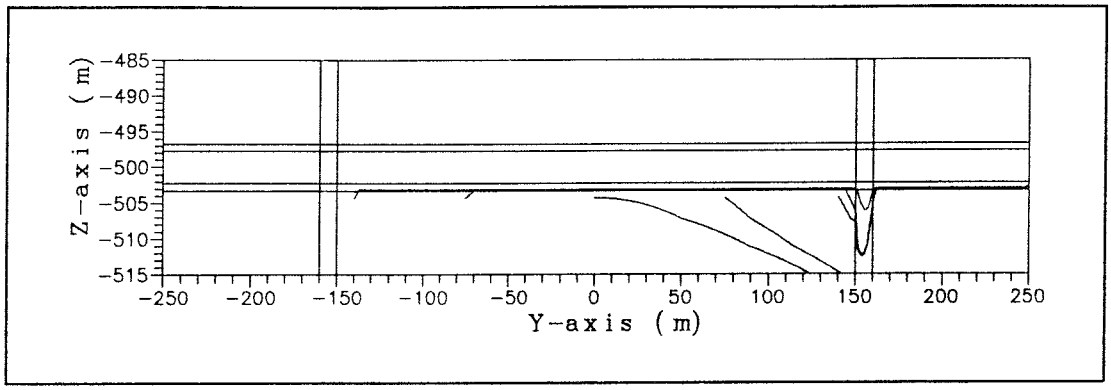

Figure 2.21 Pathlines released from the elevation of the canisters, Case L4 local model.

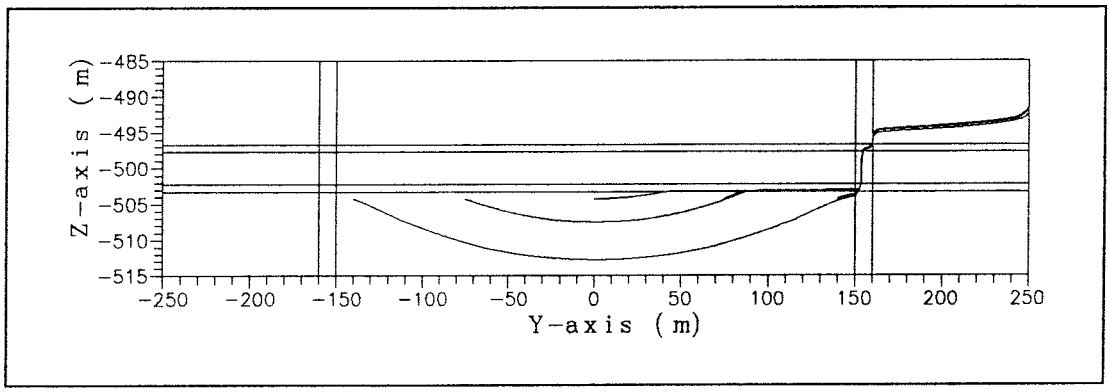

Figure 2.22 Pathlines released at the elevation of the canisters, Case L5 local model.

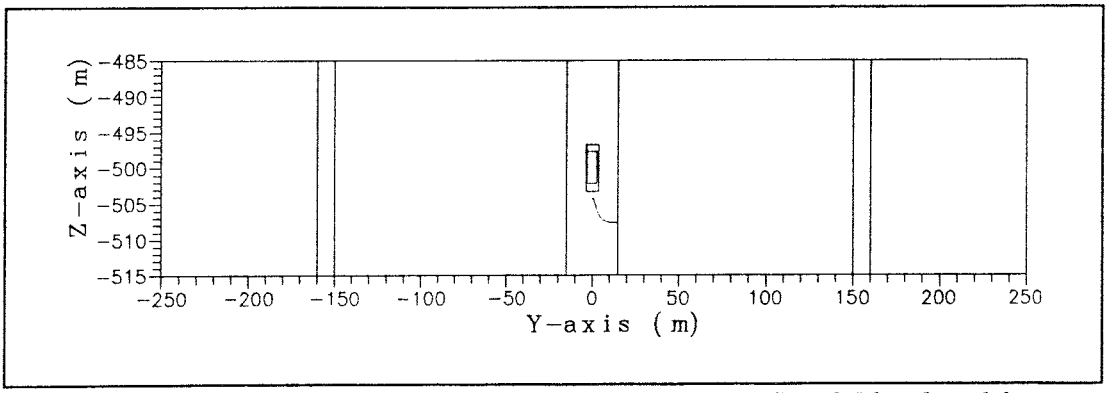

Figure 2.23 Pathlines released at the elevation of the canisters, Case L6 local model.

The groundwater Darcy velocity has been calculated along two imaginary lines, in the centre of the disturbed zone(0.5 m below the tunnel floor) and along a line which coincides with the positions of the upper portion of the waste canisters(2 m below the tunnel floor). The calculated velocities vary only little along the lines. Table 2.6 shows average values(representative values) for Cases L1-L6.

Table 2.6 Representative values of the groundwater flow rate of the disturbed zone beneath the tunnel floor and at the level of the top of the canisters.

Case	0.5m below tunnel floor [l/(m^2·yr)]	2m below tunnel floor [l/(m^2·yr)]
L 1	0.0170	0.0170
L 2	168	0.0170
L 3	0.0255	0.0255
L 4	249	0.0259
L 5	2.522	0.0256
L 6	0.0946	0.0158

From the values in Table 2.6 it can be concluded that the magnitude of the flow at the top of the canisters is only slightly changed because of the disturbed zone. The flow increase inside the disturbed zone, relative to undisturbed conditions, is approximately proportional to the permeability contrast between the rock mass and the disturbed zone for Cases L1-L5. The lowest flow magnitude is reached in Case L6 where the repository is oriented perpendicular to the regional hydraulic gradient. In a comparison between Case L4 and Case L6 it can be seen that the flow at the elevation of the canisters in the latter case is about 60% of the flow obtained when the repository is positioned parallel to the regional flow.

3 THE EFFECT OF THE DISTURBED ZONE ON THE NUCLIDE TRANSPORT

To illustrate the impact on nuclide transportation from the disturbed zone, migration calculations have been set up including the two vertical zones in the repository area(Case L3 and Case L5 in Section 2.2.3). Some relevant migration calculation data for the five particles released in the local model are shown in Table 3.1. The particle tracks have been denoted a-e where a is the particle release at the upstream end of the tunnel and e the particle release at the farthest downstream end. The geometrical description of the migration path is defined by the Darcy velocity along the particle tracks and the parameter values given in Table 3.2. The remaining parameters were derived assuming flow through planar and parallel fractures.

The fracture width is calculated as(Snow, 1968):

$$K=\frac{g}{12\nu}(\delta)^3/S$$

At ambient temperature g/12ν equals about 10^6 m^2/s.

The flow porosity ε_f is given by:

$$\varepsilon_f = \frac{\delta}{S}$$

Table 3.1 Groundwater travel time along the particle tracks, out to the vertical fracture zone (t_w, for a fracture spacing of 5 m in the disturbed zone is indicated within brackets).

L3	path length, rock (m)	t_w, rock (s)	u_0, average (m/s)	path length, disturbed zone (m)	t_w, disturbed zone (s)	u_0, average (m/s)
a	290.0	$5.70 \cdot 10^{8}$	$8.08 \cdot 10^{-13}$	-	-	-
b	225.0	$4.41 \cdot 10^{8}$	$8.09 \cdot 10^{-13}$	-	-	-
c	150.0	$2.94 \cdot 10^{8}$	$8.11 \cdot 10^{-13}$	-	-	-
d	75.0	$1.47 \cdot 10^{8}$	$8.09 \cdot 10^{-13}$	-	-	-
e	11.5	$1.97 \cdot 10^{7}$	$9.27 \cdot 10^{-13}$	-	-	-
L5						
a	290.5	$5.73 \cdot 10^{8}$	$8.05 \cdot 10^{-13}$	-	-	-
b	163.5	$3.21 \cdot 10^{8}$	$8.09 \cdot 10^{-13}$	62.0	$3.80 \cdot 10^{7}$ ($5.82 \cdot 10^{6}$)	$7.85 \cdot 10^{-11}$
c	43.0	$8.40 \cdot 10^{8}$	$8.13 \cdot 10^{-13}$	107.0	$6.40 \cdot 10^{7}$ ($9.81 \cdot 10^{6}$)	$8.03 \cdot 10^{-11}$
d	11.0	$2.14 \cdot 10^{7}$	$8.15 \cdot 10^{-13}$	64.0	$6.66 \cdot 10^{7}$ ($1.02 \cdot 10^{7}$)	$4.62 \cdot 10^{-11}$
e	10.0	$2.03 \cdot 10^{7}$	$7.81 \cdot 10^{-13}$	-	-	-

The migration calculations have been performed for the particle released at y=0, i.e. at half the tunnel length. The migration path length is defined as the length between the release point and the pathway intersection with the downstream vertical zone. In the calculation case where the disturbed zone is omitted (Case L3) the pathline follows a curved path before it reaches the vertical zone (see Figure 2.19). In the case where the disturbed zone is included(Case L5) the particle instead is led up to the disturbed zone where the particle is transported out to the vertical zone (see Figure 2.21). The calculation were made for a non-sorbing species (K_d=0) as well as for a highly sorbing species (K_d=5). The migration calculation source term is a fixed concentration of 1.0 m^{-3} at an area of 1 m^2 at the start of the pathline.

The discharge rate as a function of time is shown in Figure 3.1 and Figure 3.2 for a highly sorbing and a non-sorbing radionuclide respectively. Out of these graphs it can be concluded that the discharge rate will be higher if the rock portion of the migration path is changed to a corresponding length of the disturbed zone as the flow rate is higher here. With a fracture distance of 0.3 m in the disturbed zone, the time used for material diffusion is in the same order of magnitude as the break-through time for the case without the disturbed zone. The break-through times can be compared

Table 3.2 Migration calculation parameters.

	Undisturbed rock	Disturbed zone
ε_f (Derived according to above)	$1.5847 \cdot 10^{-6}$	$4.81 \cdot 10^{-5}$ ($7.37 \cdot 10^{-6}$)
ε_p (Assumed)	$2.0 \cdot 10^{-3}$	$2.0 \cdot 10^{-3}$
δ (Derived according to above) (m)	$7.94 \cdot 10^{-6}$ m	$1.44 \cdot 10^{-5}$ ($3.68 \cdot 10^{-5}$)
S (Assumed) (m)	5.0 m	0.3 (5.0)
Pe (Calcul. for a part of the path)	2.0	2.0
$\rho_{rock\ mass}$	2700 kg/m^3	2700 kg/m^3
D_e	$5 \cdot 10^{-14}$ m^2/s	$5 \cdot 10^{-14}$ m^2/s
K (Input in hydraulic calculations)	$1 \cdot 10^{-10}$ m/s	$1 \cdot 10^{-8}$ m/s

with e.g. the time it takes for the radionuclides to diffuse into the rock matrix. Such diffusion times defined as the time it takes for the break-through curve to rise to C/C_0=0.5 are given in Table 3.3. The time to full penetration using a 5 m fracture spacing is significantly longer than the migration time in the flow tube indicating that the rock matrix sorption capacity never is fully utilized in this case. For a fracture spacing of 0.3 m, however, the rock matrix would be fully saturated. This shows as a steeper break-through curve in Figures 3.1 and 3.2. In fact, at very small concentrations the curve for rock matrix only appears before the curve for 0.3 m spacing in the disturbed zone(not visible in the figures).

Table 3.3 Penetration time in a case where C/C_0=0.5 in a semiinfinite matrix where $D_e=5.0 \cdot 10^{-14} m^2/s$ and the porosity=$2 \cdot 10^{-3}$

	0.3 m fracture spacing	5.0 m fracture spacing
K_d=0.0	$9.89 \cdot 10^{8}$ s	$2.75 \cdot 10^{11}$ s
K_d=5.0	$6.66 \cdot 10^{15}$ s	$1.85 \cdot 10^{18}$ s

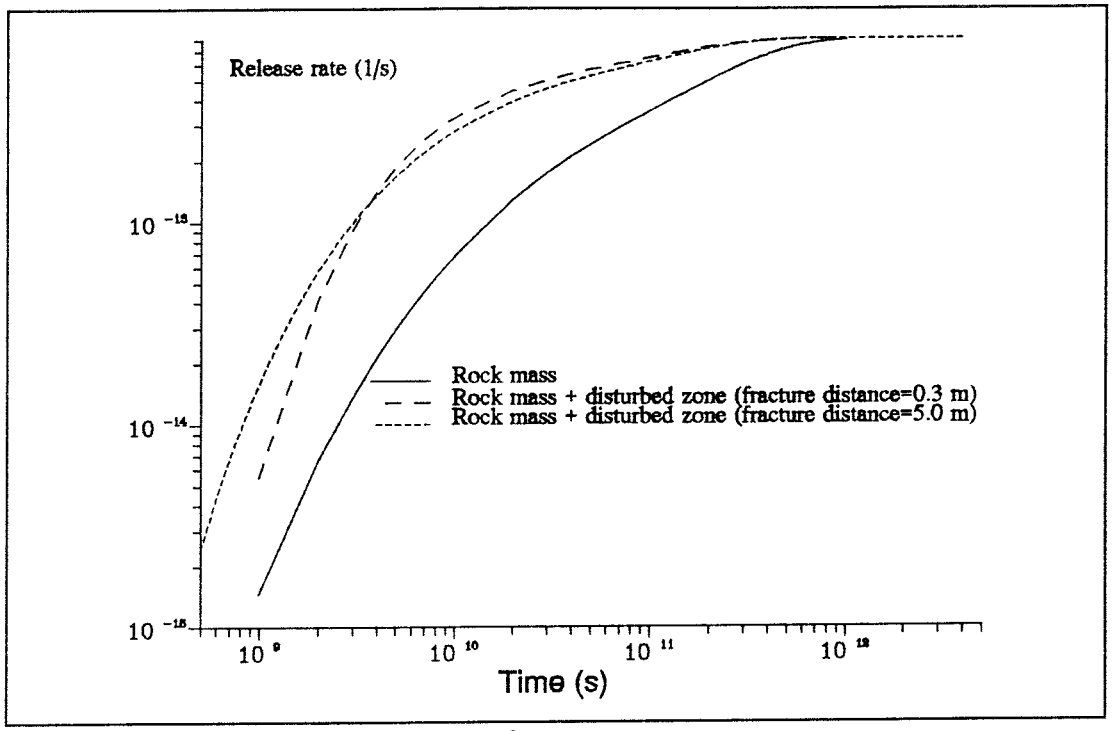

Figure 3.1 Release rate, Pathline c, K_d=0

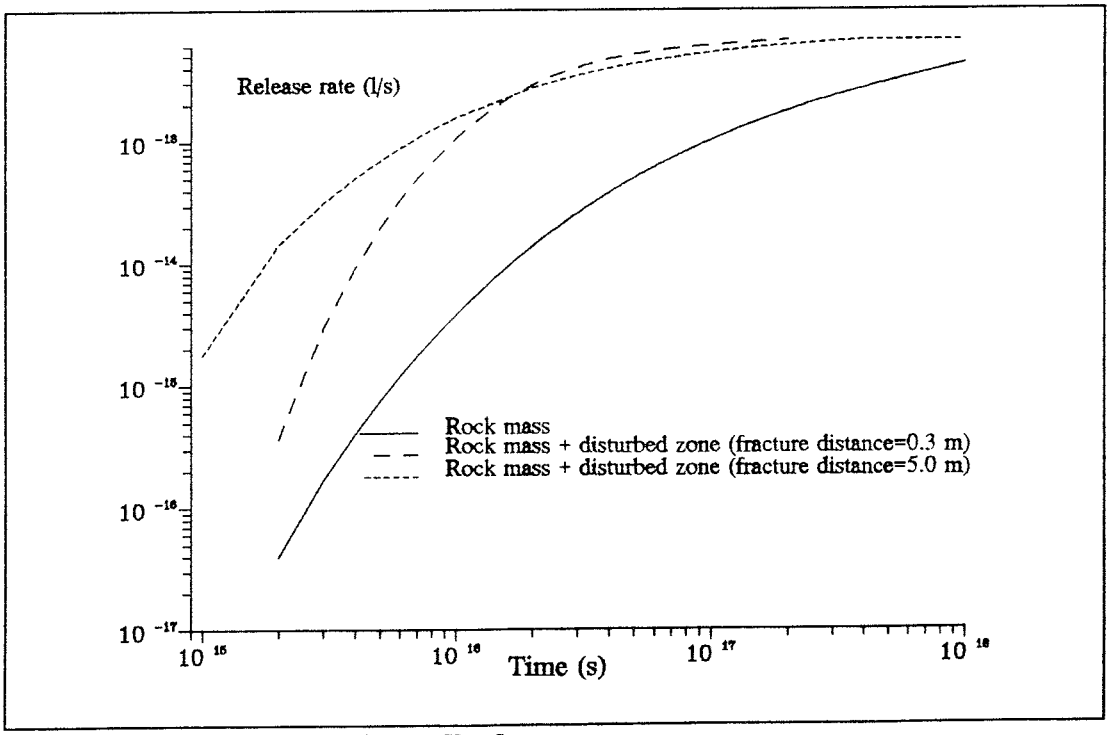

Figure 3.2. Release rate, Pathline c, K_d=5

Comparing the case without a disturbed zone and the case with a disturbed zone using a fracture distance of 0.3 m, the break-through appears slightly earlier without disturbed zone. The reason for this is the shorter transit time for the groundwater - $2.94 \cdot 10^8$s through the rock compared to $9 \cdot 10^8$s through rock plus disturbed zone. Soon after initial penetration the rock matrix in the disturbed zone will become fully permeated and will not contribute any further to the delay of nuclide release. Also the larger diffusion area into the rock matrix for the undisturbed rock (see Table 3.4.) will further slow down the release in the scenario without a disturbed zone compared to the case with a disturbed zone.

For a fracture spacing of 5 m in the disturbed zone the discharge rate is higher than without the zone at all times. The release rate at stationary conditions is equivalent in the three cases since it only depends on the water flow at the beginning of the migration path which is almost identical in all cases. In reality the effect derived from the disturbed zone depends very much on the fracture geometry and the groundwater flow. Parameter values used in this report, in particular data used for flow and diffusion geometry should be considered as assumptions. The purpose with these parameter variations has been to find the parameters to which the migration is sensitive.

Table 3.4 Specific area available for diffusion into rock matrix

	Available diffusion area (m^2/m^3 fracture volume)
Undisturbed rock	$1.26 \cdot 10^5$
Disturbed zone, S=5m	$2.72 \cdot 10^4$
Disturbed zone, S=0.3m	$6.94 \cdot 10^4$

4 CONCLUSIONS

In this study calculations have been performed to throw light upon the effect on the groundwater flow and the radionuclide transport from a permeable zone around the repository tunnel in a repository for nuclear waste. The influence on the groundwater flow has been studied by potential flow theory based on analytical solutions as well as by numerical calculations. The aim with the radionuclide transport calculations has been to illustrate possible effects on break-through times etc from the disturbed zone.

The flow rate in the disturbed zone is strongly dependent on the orientation of the tunnels relative to the flow field. A maximum flow rate enhancement of a factor 2 relative to the surrounding rock mass is obtained if the flow direction is perpendicular to the principal axis of the tunnel. If the main flow is parallel to the tunnel axis the flow increase reached is almost proportional to the permeability contrast between the disturbed zone and the surrounding rock. The water needed for such flow increase is collected from a large area upstream from the tunnel. The flow around the canisters, in the area beneath the disturbed zone, is only affected marginally by the disturbed zone.

If the disturbed zone is intersected by vertical or subvertical zones, a U-tube situation can be developed where the water is transported downwards through one fracture zone, horizontally by the disturbed zone, and upwards to the discharge area at the ground surface via the second fracture zone. Calculations made for such conditions yield a flow rate increase of about 50% in the

disturbed zone. The limited geometric extent of the disturbed zone which disables an unrestricted water uptake, is probably the explanation to the fact that the flow rate increase is relatively limited.

The flow direction beneath the tunnels, i.e. around the canisters, varies according to the position and the modelling assumptions. In the case where the repository tunnel is oriented perpendicular to the regional flow the pathlines from the canister area do not reach the disturbed zone since the influence from the disturbed zone under these conditions is limited. On the other hand in the case where the tunnel is oriented parallel to the regional flow, at least some of the pathlines will reach the disturbed zone. At high permeability contrast between rock mass and disturbed zone most of the pathlines will reach the zone. It must be made clear that the calculations performed are based on the assumption that the rock mass as well as the disturbed zone can be considered as a porous medium. If the water flows in discrete fractures of statistically distributed orientations, pathways from the canister positions to the disturbed zone can not be excluded from any canister position along the tunnel.

The calculations performed indicate that the disturbed zone is of significant importance. It is not possible with today's knowledge to exclude the possibility of transport of radionuclides from the canister positions to the disturbed zone. This becomes evident if axial diffusion in the deposition holes is considered. If the radionuclides reach the disturbed zone and the tunnel is oriented parallel to the main flow direction, the transport velocity is probably higher in the zone than in the undisturbed rock. In the calculations performed, considerations have been taken to fracture expansion in the disturbed zone corresponding to rock stress redistribution, by assuming a higher fracture frequency (3 fractures per metre in the zone and 0.2 fractures per metre in the undisturbed rock). Accordingly the difference in the nuclide travel time in the zone and the rock is smaller compared to the difference in Darcy velocity as the accessible retention capacity is higher in the zone than in the rock.

As a consequence of the introduction of the disturbed zone, it is recommended that the near-field modelling strategy is reviewed. In particular the possibility of axial diffusion in the deposition holes ought to be considered. Furthermore it should be clarified how the conductive fracture frequency or rather the accessible wetted fracture area, is affected by blasting damages and the stress redistribution. Also chemical factors, such as sorption properties of fresh fractures, the time aspect of fracture ageing together with a possible redox front extending into the disturbed zone should be discussed.

5 REFERENCES

Carslaw H.S. and J.C. Jaeger,
Conduction of Heat in Solids, 2nd. ed.,
Oxford Univ. Press, New York, 1959

Pusch, Roland
Radionuclide transport paths in the near field - A KBS-3 concept study
SKB TR 90-32, Clay Technology AB and Lund Univ. of Technology, July 1990

Snow, D.T.
Rock Fracture Spacings, Openings and Porosities,
J. Soil. Mech. Found. Div. Amer. Soc. Civ. Eng, 94(SM1), 73, 1968

6 LIST OF SYMBOLS

a,b,c	Half axises along the x, y and z direction in a prolate spheroid
δ	Fracture aperture (m)
C	Concentration in liquid phase ($1/m^3$)
C_0	Initial concentration in liquid phase, boundary concentration
D	Dispersion coefficient (m^2/s)
D_e	Effective diffusion coefficient; $D_p \cdot \varepsilon_p$ (m^2/s)
D_p	Pore diffusion coefficient (m^2/s)
g	Acceleration of gravity (m^2/s)
K	Hydraulic conductivity (m/s)
K'	Hydraulic conductivity for the disturbed zone (m/s)
K_d	Mass sorption coefficient (m^3/kg)
K_{eff}	Effective hydraulic conductivity (m/s)
l	Characteristic length
Pe	Peclet number: $u \cdot l/D$
Q	Flow rate (m^3/m^2,s)
Q'	Flow rate in within an area with the hydraulic conductivity K'
S	Fracture spacing (m)
t_w	Groundwater travel time (s)
u	Linear velocity, flow velocity in the fractures (m/s)
u_0	Darcy velocity (m^3/m^2,s)
ε_f	Flow porosity (m^2/m^2)
ε_p	Porosity accessible for diffusion (m^3/m^3)
ρ	Density (kg/m^3)
ν	Kinematic viscosity (m^2/s)

List of SKB reports

Annual Reports

1977-78
TR 121
KBS Technical Reports 1 – 120
Summaries
Stockholm, May 1979

1979
TR 79-28
The KBS Annual Report 1979
KBS Technical Reports 79-01 – 79-27
Summaries
Stockholm, March 1980

1980
TR 80-26
The KBS Annual Report 1980
KBS Technical Reports 80-01 – 80-25
Summaries
Stockholm, March 1981

1981
TR 81-17
The KBS Annual Report 1981
KBS Technical Reports 81-01 – 81-16
Summaries
Stockholm, April 1982

1982
TR 82-28
The KBS Annual Report 1982
KBS Technical Reports 82-01 – 82-27
Summaries
Stockholm, July 1983

1983
TR 83-77
The KBS Annual Report 1983
KBS Technical Reports 83-01 – 83-76
Summaries
Stockholm, June 1984

1984
TR 85-01
Annual Research and Development Report 1984
Including Summaries of Technical Reports Issued during 1984. (Technical Reports 84-01 – 84-19)
Stockholm, June 1985

1985
TR 85-20
Annual Research and Development Report 1985
Including Summaries of Technical Reports Issued during 1985. (Technical Reports 85-01 – 85-19)
Stockholm, May 1986

1986
TR 86-31
SKB Annual Report 1986
Including Summaries of Technical Reports Issued during 1986
Stockholm, May 1987

1987
TR 87-33
SKB Annual Report 1987
Including Summaries of Technical Reports Issued during 1987
Stockholm, May 1988

1988
TR 88-32
SKB Annual Report 1988
Including Summaries of Technical Reports Issued during 1988
Stockholm, May 1989

1989
TR 89-40
SKB Annual Report 1989
Including Summaries of Technical Reports Issued during 1989
Stockholm, May 1990

Technical Reports

List of SKB Technical Reports 1991

TR 91-01
Description of geological data in SKB's database GEOTAB
Version 2
Stefan Sehlstedt, Tomas Stark
SGAB, Luleå
January 1991

TR 91-02
Description of geophysical data in SKB database GEOTAB
Version 2
Stefan Sehlstedt
SGAB, Luleå
January 1991

TR 91-03
1. The application of PIE techniques to the study of the corrosion of spent oxide fuel in deep-rock ground waters
2. Spent fuel degradation
R S Forsyth
Studsvik Nuclear
January 1991

TR 91-04
Plutonium solubilities
I Puigdomènech[1], J Bruno[2]
[1]Enviromental Services, Studsvik Nuclear, Nyköping, Sweden
[2]MBT Tecnologia Ambiental, CENT, Cerdanyola, Spain
February 1991

TR 91-05
Description of tracer data in the SKB database GEOTAB
SGAB, Luleå
April, 1991

TR 91-06
Description of background data in the SKB database GEOTAB Version 2
Ebbe Eriksson, Stefan Sehlstedt
SGAB, Luleå
March 1991

TR 91-07
Description of hydrogeological data in the SKB's database GEOTAB Version 2
Margareta Gerlach[1], Bengt Gentzschein[2]
[1]SGAB, Luleå
[2]SGAB, Uppsala
April 1991

TR 91-08
Overview of geologic and geohydrologic conditions at the Finnsjön site and its surroundings
Kaj Ahlbom[1], Sven Tirén[2]
[1]Conterra AB
[2]Sveriges Geologiska AB
January 1991

TR 91-09
Long term sampling and measuring program. Joint report for 1987, 1988 and 1989. Within the project: Fallout studies in the Gideå and Finnsjö areas after the Chernobyl accident in 1986
Thomas Ittner
SGAB, Uppsala
December 1990

TR 91-10
Sealing of rock joints by induced calcite precipitation. A case study from Bergeforsen hydro power plant
Eva Hakami[1], Anders Ekstav[2], Ulf Qvarfort[2]
[1]Vattenfall HydroPower AB
[2]Golder Geosystem AB
January 1991